

1 **Enhancement of secondary organic aerosol formation and its**  
2 **oxidation state by SO<sub>2</sub> during photooxidation of 2-methoxyphenol**

3 Changgeng Liu<sup>1,2,a</sup>, Tianzeng Chen<sup>1,4,a</sup>, Yongchun Liu<sup>3,\*</sup>, Jun Liu<sup>1,4</sup>, Hong He<sup>1,4,5,\*</sup>, Peng  
4 Zhang<sup>1,4</sup>

5 <sup>1</sup>State Key Joint Laboratory of Environment Simulation and Pollution Control,  
6 Research Center for Eco-Environmental Sciences, Chinese Academy of Sciences,  
7 Beijing 100085, China

8 <sup>2</sup>School of Biological and Chemical Engineering, Panzhihua University, Panzhihua  
9 617000, China

10 <sup>3</sup>Beijing Advanced Innovation Center for Soft Matter Science and Engineering, Beijing  
11 University of Chemical Technology, Beijing 100029, China

12 <sup>4</sup>University of Chinese Academy of Sciences, Beijing 100049, China

13 <sup>5</sup>Center for Excellence in Regional Atmospheric Environment, Institute of Urban  
14 Environment, Chinese Academy of Sciences, Xiamen 361021, China

15 <sup>a</sup>These authors contributed equally to this work and should be considered as co-first  
16 authors

17 *Correspondence to:* Yongchun Liu (liuyc@buct.edu.cn) and Hong He  
18 (honghe@rcees.ac.cn)

19 **Abstract.** 2-Methoxyphenol (guaiacol) is derived from the lignin pyrolysis and taken  
20 as a potential tracer for wood smoke emissions. In this work, the effect of SO<sub>2</sub> at  
21 atmospheric levels (0–56 ppbv) on secondary organic aerosol (SOA) formation and its  
22 oxidation state during guaiacol photooxidation was investigated in the presence of  
23 various inorganic seed particles (i.e., NaCl and (NH<sub>4</sub>)<sub>2</sub>SO<sub>4</sub>). Without SO<sub>2</sub> and seed  
24 particles, SOA yields ranged from (9.46 ± 1.71)% to (26.37 ± 2.83)% and could be well  
25 expressed by a one-product model. According to the ratio of the average gas-particle  
26 partitioning timescale ( $\bar{\tau}_{g-p}$ ) over the course of experiment to the vapor wall deposition  
27 timescale ( $\tau_{g-w}$ ), the determined SOA yields were underestimated by a factor of ~2  
28 times. The presence of SO<sub>2</sub> resulted in enhancing SOA yield by 14.04–23.65%. With  
29 (NH<sub>4</sub>)<sub>2</sub>SO<sub>4</sub> and NaCl seed particles, SOA yield was enhanced by 23.07% and 29.57%,  
30 respectively, which further increased significantly to 29.78–53.43% in the presence of  
31 SO<sub>2</sub>, suggesting that SO<sub>2</sub> and seed particles have a synergetic contribution to SOA  
32 formation. The decreasing trend of  $\bar{\tau}_{g-p} / \tau_{g-w}$  ratio in the presence of seed particles and  
33 SO<sub>2</sub> suggested that more SOA-forming vapors were partitioned onto particle phase,  
34 consequently increasing SOA yields. It should be noted that SO<sub>2</sub> was found to be in  
35 favor of increasing the carbon oxidation state (OS<sub>C</sub>) of SOA, indicating that the  
36 functionalization reaction or the partitioning of highly oxidized products onto particles  
37 should be more dominant than oligomerization reaction. In addition, the average N/C  
38 ratio of SOA was 0.037, which revealed that NO<sub>x</sub> participated in the photooxidation  
39 process, consequently leading to the formation of organic N-containing compounds.

40 The experimental results demonstrate the importance of SO<sub>2</sub> on the formation processes  
41 of SOA and **organic S-containing compounds**, and also are helpful to further understand  
42 SOA formation from the atmospheric photooxidation of guaiacol and its subsequent  
43 impacts on air quality and climate.

## 44 **1 Introduction**

45 Biomass burning is considered as one of the major sources of gas and particulate  
46 pollutants in the atmosphere (Lauraguais et al., 2014b; Yang et al., 2016). Therefore, it  
47 has significant adverse impacts on regional and global air quality (Bari and Kindzierski,  
48 2016; Lelieveld et al., 2001), climate (Chen and Bond, 2010), and human health  
49 (Naeher et al., 2007). The chemical species emitted by biomass burning is mainly  
50 dependent on fuel source and combustion conditions (O'Neill et al., 2014). Natural  
51 wood is composed of cellulose (40–50 wt.%), hemicelluloses (25–35 wt.%), and lignin  
52 (18–35 wt.%) (Nolte et al., 2001). During the burning process, lignin pyrolysis could  
53 result in the formation of methoxyphenols, mainly including guaiacol (2-  
54 methoxyphenol), syringol (2,6-dimethoxyphenol), and their derivatives (Nolte et al.,  
55 2001; Schauer et al., 2001). Due to the high emission rate of methoxyphenols  
56 (900–4200 mg kg<sup>-1</sup> wood), methoxyphenols are considered as the potential tracers for  
57 wood burning (Hawthorne et al., 1989, 1992; Simoneit et al., 1993).

58 As a representative type of methoxyphenols, guaiacol mainly exists in the gas phase  
59 and is widely found in the atmosphere (Schauer et al., 2001). Its emission factor of  
60 wood burning is in the range of 172–279 mg kg<sup>-1</sup> wood (Schauer et al., 2001). In recent  
61 years, the reactivity of gas-phase guaiacol toward OH radicals (Coeur-Tourneur et al.,  
62 2010a), NO<sub>3</sub> radicals (Lauraguais et al., 2016; Yang et al., 2016), chlorine atom  
63 (Lauraguais et al., 2014a), and O<sub>3</sub> (El Zein et al., 2015) has been investigated,  
64 suggesting that its degradation by OH radicals and NO<sub>3</sub> radicals might be predominant

65 in the atmosphere. Meanwhile, several studies have reported the significant SOA  
66 formation from guaiacol oxidation by OH radicals, **produced from the photolysis of the**  
67 **OH precursors (i.e., H<sub>2</sub>O<sub>2</sub> and CH<sub>3</sub>ONO)** (Ahmad et al., 2017; Lauraguais et al., 2014b;  
68 Yee et al., 2013). However, SOA formation from the photooxidation of guaiacol in the  
69 presence of NO<sub>x</sub> has not been investigated **without adding the direct OH precursor,**  
70 even though it has been recently reported that the atmospheric level of NO<sub>x</sub> could reach  
71 up to close 200 ppbv in the severely polluted climate in China (Li et al., 2017).

72 Although many studies concentrated on the SOA production from the oxidation of  
73 volatile organic compounds (VOCs), the reported SOA yields showed high variability  
74 for a given precursor (Chu et al., 2016, 2017; Ge et al., 2017a; Lauraguais et al., 2012,  
75 2014b; Ng et al., 2007; Sarrafzadeh et al., 2016; Yee et al., 2013). This variability is  
76 mainly dependent on the numerous factors, e.g., pre-existing seed particles, SO<sub>2</sub> level,  
77 NO<sub>x</sub> level, humidity, and temperature. Two of the critical factors are the impacts of pre-  
78 existing seed particles and SO<sub>2</sub> level on SOA formation (Chu et al., 2016, 2017; Ge et  
79 al., 2017a). In addition, the atmospheric concentration of SO<sub>2</sub> could be up to close 200  
80 ppbv in the severely polluted atmosphere in China, and SOA from biomass burning and  
81 sulfate formation could significantly contribute to severe haze pollution (Li et al., 2017).  
82 During the transport process, smoke plumes from biomass burning would be inevitably  
83 mixed with suspended particles (e.g., (NH<sub>4</sub>)<sub>2</sub>SO<sub>4</sub> particles), SO<sub>2</sub>, and NO<sub>x</sub> in the  
84 atmosphere. However, the influences of these co-existed pollutants on the  
85 transformation of guaiacol and its SOA formation are still unclear. For these reasons,

86 the aim of this work was to investigate the SOA formation from guaiacol  
87 photooxidation in the presence of NO<sub>x</sub> in a 30 m<sup>3</sup> indoor smog chamber, as well as the  
88 effect of SO<sub>2</sub> on SOA formation with various inorganic seed particles.

## 89 **2 Experimental section**

### 90 **2.1 Smog Chamber**

91 The photooxidation experiments were performed in a 30 m<sup>3</sup> indoor smog chamber (4  
92 m (height) × 2.5 m (width) × 3 m (length)), which was built in a temperature-controlled  
93 room located at the Research Center for Eco-Environment Sciences, Chinese Academy  
94 of Sciences (RCEES-CAS). Its schematic structure is shown in Fig. S1. Briefly, 120  
95 UV lamps (365 nm, Philips TL 60/10R) were taken as the light source with a NO<sub>2</sub>  
96 photolysis rate of 0.55 min<sup>-1</sup>, which was comparable to the irradiation intensity at noon  
97 in Beijing (Chou et al., 2011). A maglev fan installed at the bottom center of the smog  
98 chamber was used to mix sufficiently the introduced gas species and seed particles.  
99 Temperature and relative humidity (RH) in the chamber were (302 ± 1) K and (39 ±  
100 1)%, respectively. Before each experiment, the chamber was flushed by purified dry  
101 zero air for ~36 h with a flow rate of 100 L min<sup>-1</sup> until the particle number concentration  
102 in the chamber was lower than 20 cm<sup>-3</sup>.

### 103 **2.2 Experimental procedures**

104 Gas-phase guaiacol was firstly introduced into the chamber by purified dry zero air  
105 flowing through the gently heated injector with a known volume of pure liquid guaiacol  
106 until guaiacol fully vaporized. Its concentration in the chamber was online monitored

107 by a **high-resolution** proton-transfer reaction time-of-flight mass spectrometer (HR-  
108 ToF-PTRMS) (Ionicon Analytik GmbH), and was calibrated by a commercial  
109 permeation tube (VICI AG INTERNATIONAL Valco Instruments Co., Inc.). When  
110 guaiacol concentration was stable, NO and SO<sub>2</sub> were introduced into the chamber by a  
111 **mass flow meter** using purified dry zero air as the carrier gas. Their concentrations were  
112 controlled by the injection time preset through the electromagnetic valve, and were  
113 measured by a NO<sub>x</sub> analyzer (Model 42i-TL, Thermo Fisher Scientific, Inc.) and a SO<sub>2</sub>  
114 analyzer (Model 43i, Thermo Fisher Scientific Inc.), respectively. In this work, the  
115 initial ratio (V/V) of guaiacol concentration to NO<sub>x</sub> concentration in the chamber was  
116 similar in all experiments (~1.2) (Tables 1 and 2). In addition, sodium chloride (NaCl)  
117 and ammonium sulfate ((NH<sub>4</sub>)<sub>2</sub>SO<sub>4</sub>) were used as the inorganic seeds. The seed aerosols  
118 in the chamber were generated by the atomization of a 0.02 M aqueous solution.  
119 Through atomization, the size distribution of seed particles peaked at 51–58 nm was  
120 achieved, with a number concentration of 10100–11400 cm<sup>-3</sup> (Table 2). After gas  
121 species and seed particles in the chamber were mixed well, the photooxidation  
122 experiment was carried out with the fan turned off. In this work, the OH concentrations  
123 in the chamber were  $(1.3\text{--}2.2) \times 10^6$  molecules cm<sup>-3</sup>, calculated based on the  
124 degradation rate ( $7.53 \times 10^{-11}$  cm<sup>3</sup> molecule<sup>-1</sup> s<sup>-1</sup>) of guaiacol with OH radicals (Coeur-  
125 Tourneur et al., 2010a). The chemicals and gas samples used in this work were  
126 described in **Supplement**.

### 127 **2.3 Data analysis**

128 The HR-ToF-PTRMS with a time resolution of 1 min was used online to measure the  
129 gas phase concentration of guaiacol, and its m/z range was 10–500 in the process of  
130 data acquisition. Before data collection, the peaks of the protonated water ( $[\text{H}_3^{18}\text{O}]^+$ )  
131 and protonated acetone ( $[\text{C}_3\text{H}_7\text{O}]^+$ ) ions at m/z 21.0246 and 59.0491 were used for mass  
132 calibration, with the aim to obtain accurate mass determination during experimental  
133 process. All data obtained by the HR-ToF-PTRMS were analyzed with the PTR-MS  
134 Viewer software (version 3.1.0, IONICON Analytik).

135 An Aerodyne high-resolution time-of-flight aerosol mass spectrometer (HR-ToF-  
136 AMS) was applied to online measure the chemical composition of particles and the non-  
137 refractory submicron aerosol mass (DeCarlo et al., 2006). For all experiments, the  
138 acquisition time of the HR-ToF-AMS was 2 min. The inlet flow rate, ionization  
139 efficiency, and particle sizing of the HR-ToF-AMS were calibrated at regular intervals,  
140 according to the standard protocols using the size-selected pure ammonium nitrate  
141 particles (Drewnick et al., 2005; Jimenez et al., 2003). All data obtained by the HR-  
142 ToF-AMS were analyzed by the ToF-AMS analysis toolkit SQUIRREL 1.57I/PIKA  
143 1.16I version, in Igor Pro version 6.37. The size distribution and concentration of  
144 particles were monitored by a scanning mobility particle sizer (SMPS), which is  
145 composed of a differential mobility analyzer (DMA) (Model 3082, TSI Inc.) and a  
146 condensation particle counter (CPC) (Model 3776, TSI Inc.). Assuming that particles  
147 are spherical and non-porous, the average particle density could be calculated to be 1.4  
148  $\text{g cm}^{-3}$  using the equation  $\rho = d_{va}/d_m$  (DeCarlo et al., 2004), where  $d_{va}$  is the mean vacuum

149 aerodynamic diameter measured by the HR-ToF-AMS and  $d_m$  is the mean volume-  
150 weighted mobility diameter measured by the SMPS. The mass concentration of  
151 particles measured by the HR-ToF-AMS was corrected by the SMPS data in this work  
152 using the same method as Gordon et al. (2014). In this work, the wall loss rate ( $k_{dep}$ ) of  
153  $(\text{NH}_4)_2\text{SO}_4$  particles could be expressed as  $k_{dep} = 4.15 \times 10^{-7} \times D_p^{1.89} + 1.39 \times D_p^{-0.88}$   
154 ( $D_p$  is the particle diameter (nm)), which was measured according to the literature  
155 method (Takekawa et al., 2003) and was used to correct the wall loss of SOA. In  
156 addition, its wall loss rate was determined at predetermined time intervals, which only  
157 had a slight change among different experiments.

## 158 **2.4 Vapor wall-loss correction**

159 Previous studies have indicated that the losses of SOA-forming vapors to chamber wall  
160 can result in the substantial and systematic underestimation of SOA (Zhang et al., 2014,  
161 2015). Therefore, SOA yields obtained in this work were also corrected by vapor wall  
162 loss. The effect of vapor wall deposition on SOA yields mainly depends on the  
163 competition between the uptake of organic vapors by aerosol particles and the chamber  
164 wall (Zhang et al., 2015). Thus, the ratio of the average gas-particle partitioning  
165 timescale ( $\bar{\tau}_{g-p}$ ) over the course of experiment to the vapor wall deposition timescale  
166 ( $\tau_{g-w}$ ) could be reasonably used to evaluate the underestimation of SOA yields. The  
167 detailed calculation of  $\bar{\tau}_{g-p}$  and  $\tau_{g-w}$  was shown in the Supplement.

## 168 **3 Results and discussion**

### 169 **3.1 SOA yields**

170 A series of experiments were conducted at different guaiacol/NO<sub>x</sub> concentrations under  
171 atmospheric pressure. The experimental conditions and results are shown in Table 1.  
172 SOA yield was calculated to be the ratio of SOA mass concentration ( $M_o$ ,  $\mu\text{g m}^{-3}$ ) to the  
173 consumed guaiacol concentration ( $\Delta[\text{guaiacol}]$ ,  $\mu\text{g m}^{-3}$ ) at the end of each experiment  
174 (Kang et al., 2007). The results showed that SOA yield was dependent on the initial  
175 guaiacol concentration. Higher precursor concentration would result in higher amount  
176 of condensable products, subsequently enhancing SOA formation (Lauraguais et al.,  
177 2012). In addition, it should be noted that SOA mass could directly affect the  
178 gas/particle partitioning via acting as the adsorption medium of oxidation products, thus  
179 higher SOA mass generally leads to higher SOA yield (Lauraguais et al., 2014b).

180 SOA yield ( $Y$ ) could be represented by a widely-used semi-empirical model based  
181 on the absorptive gas-particle partitioning of semi-volatile products, typically  
182 calculated using the following equation (Odum et al., 1996):

$$183 \quad Y = \sum_i M_o \frac{\alpha_i K_{om,i}}{1 + K_{om,i} M_o} \quad (1)$$

184 where  $\alpha_i$  is the mass-based stoichiometric coefficient for the reaction producing the  
185 semi-volatile product  $i$ ,  $K_{om,i}$  is the gas-particle partitioning equilibrium constant, and  
186  $M_o$  is the total aerosol mass concentration.

187 The yield curve for guaiacol photooxidation is shown in Fig. 1, obtained by plotting  
188 the SOA yield data in Table 1 according to Eq. (1). The yield data were accurately  
189 reproduced by a one-product model ( $R^2 = 0.97$ ), while two or more products used in the  
190 model did not significantly improve the fitting quality. The obtained values of  $\alpha_i$  and

191  $K_{om,i}$  for one-product model were  $(0.27 \pm 0.01)$  and  $(0.033 \pm 0.008) \text{ m}^3 \mu\text{g}^{-1}$ , respectively.  
192 In previous studies, the one-product model was widely applied to describe SOA yields  
193 from the oxidation of aromatic compounds including methoxyphenols (Coeur-Tourneur  
194 et al., 2010b; Lauraguais et al., 2012, 2014b). In this work, this simulation suggests that  
195 the products in SOA have similar values of  $\alpha_i$  and  $K_{om,i}$ , i.e., the obtained  $\alpha_i$  and  $K_{om,i}$   
196 are the average values. The plot shown in Fig. S2 is the relationship between  $M_o$  versus  
197  $\Delta[\text{guaiacol}]$ , of which slope (0.28) is slightly higher than  $\alpha_i$  value (0.27). This suggests  
198 that the formed low-volatile products almost completely partitioned on the particle-  
199 phase according to the theoretical partition model (Lauraguais et al., 2012, 2014b).

200 In the previous studies, the significant SOA formation from the OH-initiated  
201 reaction of guaiacol has been reported (Lauraguais et al., 2014b; Yee et al., 2013). In  
202 this work, SOA yields for guaiacol photooxidation range from  $(9.46 \pm 1.71)\%$  to  $(26.37$   
203  $\pm 2.83)\%$ , shown in Table 1. According to the ratios of  $\bar{\tau}_{g-p} / \tau_{g-w}$  (0.61–0.93), the  
204 determined SOA yields were underestimated by a factor of  $\sim 2$  times, suggesting that  
205 vapor wall loss in the chamber could significantly affect SOA formation. The similar  
206 results were reported previously by Zhang et al. (2014), who indicated that SOA yields  
207 for toluene photooxidation were substantially underestimated by factors as much as 4  
208 times, caused by vapor wall loss. As shown in Fig. 1, the vapor wall-loss corrected SOA  
209 yields were in the range of  $(15.24 \pm 0.85)\%$  to  $(50.89 \pm 2.87)\%$ , and could also be  
210 reproduced by a one-product model ( $R^2 = 0.96$ ). This range overlaps SOA yields of  
211 0.6–87% for guaiacol oxidation under high  $\text{NO}_x$  condition ( $\sim 10 \text{ ppmv NO}$ ), reported

212 by Lauraguais et al. (2014b), using CH<sub>3</sub>ONO as the OH source. Under low NO<sub>x</sub>  
213 conditions (<5 ppbv NO), SOA yields for guaiacol oxidation were in the range of  
214 44–50%, reported by Yee et al. (2013) using H<sub>2</sub>O<sub>2</sub> as the OH source and (NH<sub>4</sub>)<sub>2</sub>SO<sub>4</sub> as  
215 seed particles; they also indicated that high NO<sub>x</sub> concentration (>200 ppbv NO) played  
216 an opposite role in SOA formation. Overall, the vapor wall-loss corrected SOA yields  
217 in this work are well in agreement with those reported previously (Lauraguais et al.,  
218 2014b; Yee et al., 2013), but the determined SOA yields are much lower. Therefore, the  
219 effect of vapor wall loss on SOA formation should be seriously taken into account.

220 In addition, the average N/C ratio of SOA for guaiacol photooxidation in the  
221 presence of NO<sub>x</sub> is 0.037, calculated according to the element analysis by the HR-ToF-  
222 AMS. This indicates that NO<sub>x</sub> incorporates in guaiacol photooxidation. This  
223 phenomenon is well supported by the previous studies, which have reported that the  
224 nitro-substituted products are the main products of the OH-initiated reaction of guaiacol  
225 in the presence of NO<sub>x</sub> (Ahmad et al., 2017; Lauraguais et al., 2014b). The relative low  
226 volatility of these products could reasonably contribute to SOA formation (Duporté et  
227 al., 2016; Liu et al., 2016a). The average NO<sup>+</sup> / NO<sub>2</sub><sup>+</sup> ratio of SOA from guaiacol  
228 photooxidation is 4.08, which is higher than that (2.06–2.54) for ammonium nitrate,  
229 determined by the HR-ToF-AMS in this work. The possible explanation might be that  
230 nitro-organics and organonitrates both exist in SOA (Farmer et al., 2010; Sato et al.,  
231 2010). The relative abundance of organic N-containing compounds could be estimated  
232 from the average N/C ratio. Assuming that the oxidation products in the SOA retain 7

233 carbon atoms, the yield of organic **N-containing compounds** is 25.9%, which is the  
234 upper limit due to the possible C—C bond scission during photooxidation process.

## 235 **3.2 Effect of SO<sub>2</sub> on SOA formation**

### 236 **3.2.1 SOA yields**

237 In China, atmospheric SO<sub>2</sub> concentration is always in the range of several to dozens of  
238 ppb<sub>v</sub>, while in the severely polluted atmosphere it could be up to close 200 ppb<sub>v</sub> (Han  
239 et al., 2015; Li et al., 2017). In addition, a recent field measurement study has reported  
240 that the decrease of biogenic SOA mass concentration in the atmosphere has a positive  
241 correlation with SO<sub>2</sub> emission controls (Marais et al., 2017). Therefore, the effect of  
242 SO<sub>2</sub> at atmospheric levels on SOA formation from guaiacol photooxidation under  
243 atmospheric NO<sub>x</sub> conditions was investigated. The experimental conditions and results  
244 are shown in Table 2. The formation of SOA, sulfate, and nitrate as a function of SO<sub>2</sub>  
245 concentration for guaiacol photooxidation is shown in Fig. S3, **and the time-series**  
246 **variations in the concentrations of sulfate and nitrate are shown in Fig. S4. The decays**  
247 **of guaiacol, NO<sub>x</sub>, and SO<sub>2</sub> are shown in Fig. S5a, Fig. S6a, and Fig. S7, respectively,**  
248 **which have the similar changing trends for different experiments.** As illustrated in Fig.  
249 2, **the induction period became shorter with the increase of SO<sub>2</sub> concentration. The**  
250 **similar results caused by SO<sub>2</sub> have also been reported previously (Chu et al., 2016; Liu**  
251 **et al., 2016b). Meanwhile, M<sub>0</sub> for the experiment without SO<sub>2</sub> (Exp. 1 in Table 2)**  
252 **increased from (63.62 ± 1.71) to (71.88 ± 1.43) and (78.59 ± 2.06) μg m<sup>-3</sup>, enhanced by**  
253 **12.98% and 23.53%, respectively, when SO<sub>2</sub> concentration raised from 0 to 33 and 56**

254 ppbv. The corresponding SOA yields were  $(9.46 \pm 1.71)\%$ ,  $(21.60 \pm 1.27)\%$ , and  $(23.42$   
255  $\pm 1.80)\%$ , respectively. The similar results were reported by previous studies  
256 (Kleindienst et al., 2006; Lin et al., 2013; Liu et al., 2016b), which observed the  
257 significant enhancement of SOA yields for VOCs oxidation and the photochemical  
258 aging of gasoline vehicle exhaust in the presence of SO<sub>2</sub>.

259 As shown in Fig. 3,  $\bar{\tau}_{g-p} / \tau_{g-w}$  ratio decreased from 0.82 to 0.71 and 0.61 when SO<sub>2</sub>  
260 concentration increased from 0 to 33 and 56 ppbv. It suggests that the formed sulfate  
261 via SO<sub>2</sub> oxidation could serve as seed particles (Jaoui et al., 2008) and increase the  
262 surface areas of particles (Xu et al., 2016). These roles are favorable to partition more  
263 SOA-forming vapors onto particle phase (Zhang et al., 2014), consequently enhancing  
264 SOA yields. At the same time, as shown in Fig. S4 and Table 2, the sulfate concentration  
265 increased significantly from 7.42 to 18.89  $\mu\text{g m}^{-3}$  when SO<sub>2</sub> concentration increased  
266 from 33 to 56 ppbv. Nevertheless, the particle peak attributed to sulfate formed via SO<sub>2</sub>  
267 oxidation was not observed by the SMPS during experimental process due to the quick  
268 particle growth in the presence of organic vapors. In this work, it is difficult to  
269 completely remove trace NH<sub>3</sub> from zero air, thus the formed sulfate should be the  
270 mixture of H<sub>2</sub>SO<sub>4</sub> and (NH<sub>4</sub>)<sub>2</sub>SO<sub>4</sub>. The time-series changes in the concentration of  
271 ammonium salt at different SO<sub>2</sub> concentrations are shown in Fig. S8. Its concentration  
272 increased obviously with increasing SO<sub>2</sub> concentration, suggesting that the more  
273 amounts of (NH<sub>4</sub>)<sub>2</sub>SO<sub>4</sub> was produced. The similar results have also been reported  
274 recently by Chu et al. (2016). In addition, the surface area concentration of aerosol

275 particles at the end time **were calculated**. As shown in Table 2, the final surface area of  
276 aerosol particles formed via guaiacol photooxidation increased from  $1.25 \times 10^3$  to  $1.68$   
277  $\times 10^3$  and  $2.04 \times 10^3 \mu\text{m}^2 \text{cm}^{-3}$  when  $\text{SO}_2$  concentration increased from 0 to 33 and 56  
278 **ppbv**. The increased surface area could be in favor of outcompeting the wall loss for  
279 low-volatility vapors produced from guaiacol photooxidation, i.e., more low-volatility  
280 vapors **would** be diverted from wall loss to the particles, consequently increasing SOA  
281 yields (Kroll et al., 2007). **This is well supported by the decrease of  $\bar{\tau}_{\text{g-p}} / \tau_{\text{g-w}}$  ratio with**  
282 **increasing  $\text{SO}_2$  concentration, shown in Fig. 3.**

283 **The time-series changes in the mass concentrations of  $\text{NO}^+$  and  $\text{NO}_2^+$  are shown**  
284 **in Fig. S9a. The mass concentration of  $\text{NO}^+$  increased more quickly than that of  $\text{NO}_2^+$ ,**  
285 **and had a positive correlation with  $\text{SO}_2$  concentration. But, compared to the experiment**  
286 **without  $\text{SO}_2$ , the presence of  $\text{SO}_2$  had little impact on  $\text{NO}^+ / \text{NO}_2^+$  and N/C ratios**  
287 **obtained at the end time, shown in Fig. S9b and Fig. S10b, respectively. These ratios**  
288 **indicated that organic N-containing compounds were also produced in this system**  
289 **(Farmer et al., 2010; Sato et al., 2010).**

### 290 **3.2.2 Oxidation state of SOA**

291 The average carbon oxidation state ( $\text{OS}_\text{C} = 2\text{O}/\text{C} - \text{H}/\text{C}$ ) of OA is widely used to  
292 represent the oxidation degree of atmospheric OA, because it takes into account the  
293 saturation level of carbon atoms in the OA (Kroll et al., 2011). As shown in Table 2,  
294 increasing  $\text{SO}_2$  concentration (0–56 **ppbv**, **Exps. 1–3**) leads to the increase of  $\text{OS}_\text{C}$   
295 (0.11–0.18). **The variations in H/C, O/C, and N/C ratios as a function of irradiation time**

296 are shown in Fig. S10. In order to further identify the effect of SO<sub>2</sub> on the chemical  
297 properties of SOA, positive matrix factorization (PMF) analysis for all AMS data  
298 obtained at different SO<sub>2</sub> concentrations over the course of experiments was carried out.  
299 Two factors were obtained from the PMF analysis, and their mass spectra are shown in  
300 Fig. 4. The organic mass fraction of m/z 44 (CO<sub>2</sub><sup>+</sup>), named  $f_{44}$ , was 0.122 for Factor 2,  
301 which is higher than that (0.094) for Factor 1. Therefore, Factor 2 was tentatively  
302 assigned to the more-oxidized SOA, while Factor 1 was the less-oxidized SOA (Ulbrich  
303 et al., 2009). During the photooxidation process, these two factors had different  
304 variations as a function of irradiation time. As shown in Fig. S11, Factor 1 increased  
305 along with the reaction and then decreased, while Factor 2 had an increasing trend.  
306 Compared to Exps. 1 and 2 in Table 2, the higher fraction of Factor 2 mass obtained at  
307 56 ppbv SO<sub>2</sub> (Exp. 3 in Table 2) suggests that the formed SOA mainly consists of more-  
308 oxidized products with relatively low volatility. This is well supported by the time-  
309 series variations in the fraction of organic ion groups (CH<sup>+</sup>, CHO<sup>+</sup>, and CHO<sub>gt1</sub><sup>+</sup>) (Fig.  
310 S12a), which shows the higher fraction of CHO<sub>gt1</sub><sup>+</sup> and lower fraction of CH<sup>+</sup> obtained  
311 at higher SO<sub>2</sub> concentration, consequently resulting in higher OSC of SOA.

312 Previous studies mostly reported that the enhancement of SOA yield in the presence  
313 of SO<sub>2</sub> was ascribed to the functionalization and oligomerization reactions (Cao and  
314 Jang, 2007; Jaoui et al., 2008 ; Liu et al., 2016b; Xu et al., 2016). If the oligomerization  
315 reaction plays a predominant role in the presence of SO<sub>2</sub> which will lead to particle  
316 phase H<sub>2</sub>SO<sub>4</sub>, the carbon number of oligomers will increase but their net O/C or H/C

317 values have little change, consequently resulting in little change in the oxidation state  
318 of SOA (Chen et al., 2011). Nevertheless, we observed that SO<sub>2</sub> not only enhanced SOA  
319 yields, but also resulted in higher O<sub>Sc</sub> (Table 2 and Fig. 5). This suggests that the  
320 functionalization reaction might be predominant with SO<sub>2</sub>, which leads to higher O<sub>Sc</sub>  
321 of products with low molecular weight (MW) (Ye et al., 2018), consequently resulting  
322 in an overall increase in O<sub>Sc</sub> and SOA yields. More recently, Ye et al. (2018) also found  
323 the similar results in the ozonolysis of limonene. Fig. S13 shows the differences among  
324 the normalized mass spectra of SOA formed at different SO<sub>2</sub> concentrations. As shown  
325 in Fig. S13a, the signal fractions from the low-MW species were enhanced significantly  
326 in the presence of SO<sub>2</sub>, and were much higher than those from the high-MW species  
327 (m/z >300). The similar results were also observed in Fig. S13b when increasing SO<sub>2</sub>  
328 concentration. In other words, SO<sub>2</sub> played a more important role in the formation of  
329 organic S-containing compounds and the formation or uptake of low-MW species,  
330 compared to the formation of high-MW species (i.e., oligomers) that should be  
331 reasonably produced via the acid-catalyzed heterogeneous reactions (Cao and Jang,  
332 2007; Jaoui et al., 2008; Liu et al., 2016b; Xu et al., 2016). In this work, the conservative  
333 lower-bound concentration of organosulfates increased with the increase of SO<sub>2</sub>  
334 concentration, and was in the range of (2.1 ± 0.8) to (4.3 ± 1.7) ng m<sup>-3</sup>, calculated using  
335 the method described by Huang et al. (2015), shown in the Supplement. This  
336 concentration range is close to those derived from the atmospheric oxidation of  
337 polycyclic aromatic hydrocarbons and alkane (Meade et al., 2016; Riva et al., 2015).

338 Fig. S14 is the examples of the ions (i.e.,  $\text{CSO}^+$ ,  $\text{CH}_3\text{SO}_2^+$ , and  $\text{CH}_3\text{SO}_3^+$ ) of methyl  
339 sulfate obtained at 56 ppbv  $\text{SO}_2$  (Exp. 3 in Table 2). On the other hand, sulfuric acid  
340 formed from  $\text{SO}_2$  may be favorable of the uptake of water-soluble low-MW species  
341 (e.g., small carboxylic acids and aldehydes), which also results in the increase of  $\text{OSc}$ .  
342 This is well supported by the time-series variations in the concentrations of acetic acid  
343 at different  $\text{SO}_2$  concentrations measured by the HR-ToF-PTRMS (Fig. S15a), which  
344 shows that acetic acid concentration decreased with the increase of  $\text{SO}_2$  concentration  
345 (0–56 ppbv). These results were in good agreement with those reported by Liggio et al.  
346 (2005) and Liu et al. (2010), who observed that that the uptake of organic compounds  
347 under acidic conditions would be enhanced significantly. Recently, Huang et al. (2016)  
348 have also reported that acetic acid is present in SOA formed via  $\alpha$ -pinene ozonolysis  
349 and its uptake would increase in the presence of seed particles. In addition, Krapf et al.  
350 (2016) have indicated that peroxides in SOA are unstable and liable to decompose into  
351 volatile compounds, consequently leading to decrease SOA yield and  $\text{OSc}$ . But, Ye et  
352 al. (2018) found that the reactions of  $\text{SO}_2$  with organic peroxides were the dominant  
353 sink of  $\text{SO}_2$ , initiated by the heterogeneous uptake of  $\text{SO}_2$  under humidity condition.  
354 These reactions would result in the formation of organic S-containing compounds,  
355 consequently increasing SOA yields and  $\text{OSc}$ .

### 356 3.3 Effect of inorganic seed particles on SOA formation

357 Seed particle is one of the critical factors influencing SOA formation (Ge et al., 2017a),  
358 thus the effects of inorganic seeds (i.e.,  $\text{NaCl}$  and  $(\text{NH}_4)_2\text{SO}_4$ ) on SOA formation from

359 guaiacol photooxidation were investigated. As shown in Fig. 6, the presence of  
360 inorganic seed particles could accelerate SOA growth rate at the initial stage of  
361 photooxidation (i.e., shorten induction period), followed by the decrease of growth rate  
362 along with the reaction, because the presence of inorganic seeds could promote the  
363 condensation of SOA-forming organic products and consequently increase SOA  
364 formation (Yee et al., 2013). The results showed that  $M_0$  for the experiment without  
365 seed particles (Exp. 1 in Table 2) increased from  $(63.62 \pm 1.71)$  to  $(79.44 \pm 1.86)$  and  
366  $(84.91 \pm 2.01)$   $\mu\text{g m}^{-3}$  (Table 2), enhanced by 24.87% and 33.46%, respectively, with  
367  $(\text{NH}_4)_2\text{SO}_4$  and NaCl seed particles. The corresponding SOA yields were  $(23.31 \pm 1.59)\%$   
368 and  $(24.54 \pm 1.73)\%$ , respectively. In previous work, the similar results about the  
369 enhancements of SOA formation by NaCl and  $(\text{NH}_4)_2\text{SO}_4$  seed particles were reported  
370 in the oxidation of VOCs (Ge et al., 2017a, 2017b; Huang et al., 2013, 2017). As shown  
371 in Fig. 3,  $\bar{\tau}_{\text{g-p}} / \tau_{\text{g-w}}$  ratios with  $(\text{NH}_4)_2\text{SO}_4$  and NaCl seed particles were 0.62 and 0.54,  
372 respectively, which suggested that more SOA-forming vapors were partitioned onto  
373 particle phase in the presence of NaCl seed particles (Zhang et al., 2014), consequently  
374 resulting in relatively higher SOA yield.

375 As shown in Table 2 and Fig. 6, the SOA mass concentration in the presence of  
376 NaCl seed particles was higher than that in the presence of  $(\text{NH}_4)_2\text{SO}_4$  seed particles.  
377 In addition,  $\text{Osc}$  of SOA in the presence of NaCl seed particles is 0.29, slightly higher  
378 than that (0.20) in the presence of  $(\text{NH}_4)_2\text{SO}_4$  seed particles. Recently, it has been also  
379 reported that the presence of  $(\text{NH}_4)_2\text{SO}_4$  and  $\text{NaNO}_3$  seed particles could enhance

380 significantly the oxidation state of SOA, compared to without seed particles (Huang et  
381 al., 2016). In this work, the experimental conditions for seed experiments are almost  
382 the same (Table 2), including reactant concentration, temperature, RH, and the number  
383 and diameter of seed particles. Therefore, the differences in the yield and oxidation state  
384 of SOA were reasonably resulted from the different chemical compositions of SOA in  
385 the presence of different inorganic seeds. As shown in Figs. S12b and S12c, compared  
386 to  $(\text{NH}_4)_2\text{SO}_4$  seed particles, the higher fraction of  $\text{CHO}_{\text{gt1}}^+$  and lower fraction of  $\text{CH}^+$   
387 were obtained with NaCl seed particles, consequently resulting in higher OSc of SOA.  
388 The time-series evolution of O/C, H/C, and N/C ratios is shown in Figs. S16 and S17,  
389 which indicate that O/C ratio with NaCl seed particles is higher than that with  
390  $(\text{NH}_4)_2\text{SO}_4$  seed particles. Fig. 7 shows the mass spectra of SOA in the presence of NaCl  
391 and  $(\text{NH}_4)_2\text{SO}_4$  seed particles obtained by the HR-ToF-AMS, as well as their difference  
392 mass spectrum. As shown in Fig. 7,  $f_{44}$  for SOA in the presence of NaCl seed particles  
393 was higher than that obtained in the presence of  $(\text{NH}_4)_2\text{SO}_4$  seed particles, while the  
394 mass fractions of  $m/z$  15 ( $\text{CH}_3$ ) and 29 ( $\text{CHO}$ ) fragments were both lower. The  $m/z$  44  
395 ion ( $\text{CO}_2^+$ ) is mainly contributed from acids or acid-derived species, such as esters (Ng  
396 et al., 2011). The higher  $f_{44}$  of SOA with NaCl than  $(\text{NH}_4)_2\text{SO}_4$  seed particles suggests  
397 that the distribution of highly oxidized small carboxylic acids onto seed particles plays  
398 an important role in SOA formation, consequently resulting in higher oxidation state of  
399 SOA (Huang et al., 2016; Ng et al., 2011). Compared to  $(\text{NH}_4)_2\text{SO}_4$ , the hygroscopicity  
400 of NaCl is stronger (Ge et al., 2017a; Gysel et al., 2002). The molar ratio of  $\text{H}_2\text{O}$  to

401 NaCl is about 0.1 at 40% RH, and water is mainly adsorbed on NaCl particles (Weis  
402 and Ewing, 1999). Thus, the greater water content on the particle surface could facilitate  
403 the uptake of highly oxidized small carboxylic acids onto NaCl particles, which might  
404 be potentially explain the higher SOA oxidation state observed in the presence of NaCl  
405 seed particles (Huang et al., 2016). As shown in Fig. S15, the concentration of acetic  
406 acid in the gas phase with NaCl seed particles was lower than that with (NH<sub>4</sub>)<sub>2</sub>SO<sub>4</sub> seed  
407 particles. It suggests that the uptake of acetic acid on NaCl seed particles might be  
408 higher than that on (NH<sub>4</sub>)<sub>2</sub>SO<sub>4</sub> seed particles under the similar experimental conditions  
409 (i.e., NO<sub>x</sub> and guaiacol concentrations, temperature, and RH). Moreover, the adsorbed  
410 acid products would also generate H<sup>+</sup> ions, which could catalyze heterogeneous  
411 reactions to produce more-oxidized products or oligomers with relatively low volatility  
412 (Fig. S18), consequently resulting in the enhancement of SOA formation (Huang et al.,  
413 2013, 2017; Cao and Jang, 2007; Jaoui et al., 2008; Liu et al., 2016b; Xu et al., 2016).

414 In addition, the possible formation of Cl atoms from the photolysis of nitryl  
415 chloride ( $\text{ClNO}_2 \xrightarrow{h\nu} \text{Cl} + \text{NO}_2$ ,  $k_1 = \sim 10^{-4} \text{ s}^{-1}$ ) (Mielke et al., 2011) and the reaction  
416 of OH radical with Cl<sup>-</sup> ( $\text{Cl}^- + \text{OH} \rightarrow \text{Cl} + \text{OH}^-$ ,  $k_2 = \sim 10^9 \text{ M}^{-1} \text{ s}^{-1}$ ) (Fang et al., 2014)  
417 would also initiate a series of reactions to oxidize SOA composition, which might be  
418 another reason for higher OSC observed with NaCl seed particles. According to the rate  
419 constant ( $10^9 \text{ M}^{-1} \text{ s}^{-1}$ ) (Fang et al., 2014), the uptake coefficient ( $3.4 \times 10^{-3}$ ) of OH  
420 radicals on NaCl particles (Park et al., 2008), and the concentrations of OH radicals and  
421 Cl<sup>-</sup>, the concentration of Cl atoms produced from the reaction of OH radical with Cl<sup>-</sup>

422 was estimated to be less than 38 molecules  $\text{cm}^{-3}$ , which was much higher than that from  
423 the photolysis of  $\text{ClNO}_2$  due to the slow photolysis rate constant of  $\sim 10^{-4} \text{ s}^{-1}$  (Mielke  
424 et al., 2011). Compared to OH concentration in the chamber, the oxidation of SOA  
425 composition by Cl atoms should be insignificant.

### 426 3.4 Synergetic effect of $\text{SO}_2$ and inorganic seed particles on SOA formation

427 According to the former results obtained in this work, it is clearly known that  $\text{SO}_2$  and  
428 inorganic seed particles both have a positive role in enhancing SOA formation.  
429 Therefore, their possible synergetic effects on SOA formation were investigated.  
430 Considering the experiments performed under the comparable conditions (Table 2), the  
431 results should be reasonably reliable. The decays of guaiacol,  $\text{NO}_x$ , and  $\text{SO}_2$  are shown  
432 in Fig. S5, Fig. S6, and Fig. S7, respectively, which have the similar changing trends  
433 for different experiments. Fig. S19 shows the time-series evolution in the sulfate  
434 concentration in the presence of different  $\text{SO}_2$  concentrations and seed particles, which  
435 indicates that sulfate concentration is dependent on  $\text{SO}_2$  concentration. As shown in Fig.  
436 8, the addition of  $\text{SO}_2$  into the chamber in the presence of inorganic seed particles  
437 significantly promoted SOA formation from guaiacol photooxidation, but had an  
438 ignorable impact on the induction period. When  $\text{SO}_2$  concentration raised from 0 to 30  
439 and 54 ppbv in the presence of NaCl seed particles,  $M_o$  increased from  $(63.62 \pm 1.71)$   
440 to  $(90.89 \pm 2.28)$  and  $(98.86 \pm 2.11) \mu\text{g m}^{-3}$ , enhanced by 42.86% and 55.39%,  
441 respectively, and the corresponding SOA yields were  $(26.78 \pm 1.97)\%$  and  $(29.06 \pm$   
442  $1.82)\%$ . For  $(\text{NH}_4)_2\text{SO}_4$  seed particles,  $M_o$  increased from  $(63.62 \pm 1.71)$  to  $(84.35 \pm$

443 2.09) for 33 ppbv SO<sub>2</sub> and (89.92 ± 2.31) μg m<sup>-3</sup> for 54 ppbv SO<sub>2</sub>, enhanced by 32.58%  
444 and 41.34%, respectively, and the corresponding SOA yields were (24.58 ± 1.78)% and  
445 (26.37 ± 1.98)%. As shown in Fig. 3,  $\bar{\tau}_{g-p} / \tau_{g-w}$  ratio had a decreasing trend when  
446 increasing SO<sub>2</sub> concentration in the presence of seed particles, suggesting that the  
447 underestimation of SOA yields caused by vapor wall loss was weakened significantly  
448 because of the additional sulfate formed from SO<sub>2</sub> oxidation. Thus, inorganic seed  
449 particles and SO<sub>2</sub> have a synergistic effect on SOA formation.

450 As shown in Table 2 and Fig. 5, it should be noted that O<sub>Sc</sub> of SOA increased in  
451 the presence of SO<sub>2</sub>, which was well supported by the time-series variations in H/C,  
452 O/C, and N/C ratios at different SO<sub>2</sub> concentrations with NaCl and (NH<sub>4</sub>)<sub>2</sub>SO<sub>4</sub> as seed  
453 particles, shown in Figs. S16 and S17. In addition, as shown in Figs. S12b and S12c,  
454 the higher fraction of CHO<sub>gt1</sub><sup>+</sup> and lower fraction of CH<sup>+</sup> were obtained at higher SO<sub>2</sub>  
455 concentration, consequently resulting in higher O<sub>Sc</sub> of SOA. Fig. S20 shows the mass  
456 spectra of SOA with NaCl and (NH<sub>4</sub>)<sub>2</sub>SO<sub>4</sub> as seed particles at different SO<sub>2</sub>  
457 concentrations obtained by the HR-ToF-AMS. As illustrated in Fig. S20, SO<sub>2</sub> addition  
458 was in favor of increasing the value of  $f_{44}$ , suggesting that more products with higher  
459 O<sub>Sc</sub> are produced by the functionalization reaction (Ye et al., 2018). Meanwhile, Table  
460 2 shows that the final surface area of aerosol particles increased in the presence of SO<sub>2</sub>,  
461 which played a positive role in diverting more low-volatility vapors from wall loss to  
462 the particles, consequently enhancing SOA yields (Kroll et al., 2007). In addition, the  
463 presence of inorganic seeds could promote the condensation of SOA-forming organic

464 products and the heterogeneous uptake of SO<sub>2</sub> (Yee et al., 2013), providing favorable  
465 conditions for the following oxidation reactions. Meanwhile, the higher hygroscopicity  
466 of NaCl than (NH<sub>4</sub>)<sub>2</sub>SO<sub>4</sub> might be helpful to dissolve more acid substances on NaCl  
467 particle surface (e.g., H<sub>2</sub>SO<sub>4</sub> and organic acid), especially in the presence of SO<sub>2</sub>. This  
468 hypothesis could be supported by the variations in acetic acid concentration in the  
469 presence of different seed particles and SO<sub>2</sub> concentrations (Fig. S15), which shows  
470 that acetic acid concentration decreased with the increase of SO<sub>2</sub> concentration (0–54  
471 ppbv). The dissolved acid compounds might be helpful to catalyze heterogeneous  
472 reactions (Cao and Jang, 2007; Huang et al., 2013, 2017; Jaoui et al., 2008; Liu et al.,  
473 2016b; Xu et al., 2016). Figs. S21 and S22 show the differences among the normalized  
474 mass spectra of SOA formed at different SO<sub>2</sub> concentrations with various seed particles.  
475 The results indicated that the signal fractions from the low-MW species increased  
476 significantly in the presence of SO<sub>2</sub>, and were much higher than those from the high-  
477 MW species (m/z >300). Compared to Exps. 2 and 3 in Table 2 with no seed particles,  
478 the conservative lower-bound concentrations of organosulfates formed with seed  
479 particles were similar and in the range of (2.2 ± 0.7) to (4.6 ± 1.8) ng m<sup>-3</sup>, which might  
480 be caused by the similar SO<sub>2</sub> concentrations applied for experiments. With NaCl and  
481 (NH<sub>4</sub>)<sub>2</sub>SO<sub>4</sub> as seed particles, SOA yields and OSC both increased with the increase of  
482 SO<sub>2</sub>, suggesting that the functionalization reaction should be more dominant than  
483 oligomerization reaction during photooxidation process.

#### 484 **4 Conclusions and atmospheric implications**

485 In this work, SOA formation from guaiacol photooxidation in the presence of NO<sub>x</sub> was  
486 investigated in a 30 m<sup>3</sup> smog chamber. SOA yields for guaiacol photooxidation were in  
487 the range of (9.46 ± 1.71)% to 26.37 ± 2.83)%, and could be expressed well by a one-  
488 product model. These yields were underestimated by a factor of ~2 times according to  
489  $\bar{\tau}_{g-p} / \tau_{g-w}$  ratios. The presence of SO<sub>2</sub> could increase SOA yield and OS<sub>C</sub>, indicating that  
490 the functionalization reaction should be more dominant than oligomerization reaction.  
491 Meanwhile, the similar effect of SO<sub>2</sub> was also observed with NaCl and (NH<sub>4</sub>)<sub>2</sub>SO<sub>4</sub> seed  
492 particles. But, SOA yield and OS<sub>C</sub> in the presence of NaCl seed particles were both  
493 slightly higher than those in the presence of (NH<sub>4</sub>)<sub>2</sub>SO<sub>4</sub> seed particles. In addition, the  
494 results indicated the synergetic contribution of SO<sub>2</sub> and inorganic seed particles to SOA  
495 formation. The decreasing trend of  $\bar{\tau}_{g-p} / \tau_{g-w}$  ratio in the presence of seed particles and  
496 SO<sub>2</sub> suggested that more SOA-forming vapors were partitioned onto particle phase,  
497 consequently increasing SOA yields. The average N/C ratio (0.037) of SOA suggested  
498 that NO<sub>x</sub> participated in the process of guaiacol photooxidation, resulting in the  
499 formation of organic N-containing compounds.

500 The significant SOA formation from guaiacol photooxidation at the atmospheric  
501 levels of SO<sub>2</sub> and NO<sub>x</sub> in this work suggests that it should pay more attention to the SOA  
502 formation from biomass burning and its subsequent effects on haze evolution,  
503 especially in China with nationwide biomass burning, because recent studies have  
504 indicated that SOA formed from biomass burning plays an important role in haze  
505 pollution in China (Ding et al., 2017; Li et al., 2017). In addition, the results imply that

506 the oxidation of SO<sub>2</sub> and VOCs should be tightly combined, and SO<sub>2</sub> has a direct impact  
507 on the chemistry of SOA formation. Although guaiacol concentrations in the chamber  
508 study are higher than those in the ambient atmosphere, the results obtained in this work  
509 could provide new information for SOA formation from the photooxidation of  
510 methoxyphenols, and might be useful for SOA modeling, especially for air quality  
511 simulation modeling of the specific regions experiencing serious pollution caused by  
512 fine particulate matter. In addition, the results would help to further understand the  
513 photochemical aging process of smoke plumes from biomass burning in the atmosphere.

#### 514 **Data availability**

515 The experimental data are available upon request to the corresponding authors.

#### 516 **Competing interests**

517 The authors declare that they have no conflict of interest.

#### 518 **Acknowledgements**

519 This work was financially supported by the National Key R&D Program of China  
520 (2016YFC0202700), the National Natural Science Foundation of China (21607088 and  
521 41877306), China Postdoctoral Science Foundation funded project (2017M620071),  
522 the Applied Basic Research Project of Science and Technology Department of Sichuan  
523 Province (2018JY0303) and Key Research Program of Frontier Sciences, CAS  
524 (QYZDB-SSW-DQC018). Liu Y. would like to thank Beijing University of Chemical  
525 Technology for financial supporting. Authors would also acknowledge the experimental

526 help provided by Dr. Xiaolei Bao from Hebei Provincial Academy of Environmental  
527 Sciences, Shijiazhuang, China.

## 528 **References**

- 529 Ahmad, W., Coeur, C., Tomas, A., Fagniez, T., Brubach, J.-B., and Cuisset, A.: Infrared  
530 spectroscopy of secondary organic aerosol precursors and investigation of the  
531 hygroscopicity of SOA formed from the OH reaction with guaiacol and syringol,  
532 *Appl. Opt.*, 56, E116-E122, doi: 10.1364/ao.56.00e116, 2017.
- 533 Bari, M. A., and Kindzierski, W. B.: Fine particulate matter (PM<sub>2.5</sub>) in Edmonton,  
534 Canada: Source apportionment and potential risk for human health, *Environ.*  
535 *Pollut.*, 218, 219-229, doi: 10.1016/j.envpol.2016.06.014, 2016.
- 536 Cao, G., and Jang, M.: Effects of particle acidity and UV light on secondary organic  
537 aerosol formation from oxidation of aromatics in the absence of NO<sub>x</sub>, *Atmos.*  
538 *Environ.*, 41, 7603-7613, doi: 10.1016/j.atmosenv.2007.05.034, 2007.
- 539 **Chen, Q., Liu, Y., Donahue, N. M., Shilling, J. E., and Martin S. T.: Particle-phase**  
540 **chemistry of secondary organic material: Modeled compared to measured O:C and**  
541 **H:C elemental ratios provide constraints, *Environ. Sci. Technol.*, 45, 4763-4770,**  
542 **doi: 10.1021/es104398s, 2011.**
- 543 Chen, Y., and Bond, T. C.: Light absorption by organic carbon from wood combustion,  
544 *Atmos. Chem. Phys.*, 10, 1773-1787, doi: 10.5194/acp-10-1773-2010, 2010.
- 545 Chou, C. C. K., Tsai, C. Y., Chang, C. C., Lin, P. H., Liu, S. C., and Zhu, T.:  
546 Photochemical production of ozone in Beijing during the 2008 Olympic Games,  
547 *Atmos. Chem. Phys.*, 11, 9825-9837, doi: 10.5194/acp-11-9825-2011, 2011.
- 548 Chu, B., Zhang, X., Liu, Y., He, H., Sun, Y., Jiang, J., Li, J., and Hao, J.: Synergetic  
549 formation of secondary inorganic and organic aerosol: Effect of SO<sub>2</sub> and NH<sub>3</sub> on  
550 particle formation and growth, *Atmos. Chem. Phys.*, 16, 14219-14230, doi:  
551 10.5194/acp-16-14219-2016, 2016.
- 552 Chu, B., Liggiio, J., Liu, Y., He, H., Takekawa, H., Li, S.-M., and Hao, J.: Influence of  
553 metal-mediated aerosol-phase oxidation on secondary organic aerosol formation  
554 from the ozonolysis and OH-oxidation of  $\alpha$ -pinene, *Sci. Rep.*, 7, 40311, doi:  
555 10.1038/srep40311, 2017.
- 556 Coeur-Tourneur, C., Cassez, A., and Wenger, J. C.: Rate coefficients for the gas-phase  
557 reaction of hydroxyl radicals with 2-methoxyphenol (guaiacol) and related  
558 compounds, *J. Phys. Chem. A*, 114, 11645-11650, doi: 10.1021/jp1071023, 2010a.
- 559 Coeur-Tourneur, C., Foulon, V., and Lareal, M.: Determination of aerosol yields from  
560 3-methylcatechol and 4-methylcatechol ozonolysis in a simulation chamber,  
561 *Atmos. Environ.*, 44, 852-857, doi: 10.1016/j.atmosenv.2009.11.027, 2010b.
- 562 DeCarlo, P. F., Slowik, J. G., Worsnop, D. R., Davidovits, P., and Jimenez, J. L.: Particle  
563 morphology and density characterization by combined mobility and aerodynamic

564 diameter measurements. Part 1: Theory, *Aerosol Sci. Technol.*, 38, 1185-1205, doi:  
565 10.1080/027868290903907, 2004.

566 DeCarlo, P. F., Kimmel, J. R., Trimborn, A., Northway, M. J., Jayne, J. T., Aiken, A. C.,  
567 Gonin, M., Fuhrer, K., Horvath, T., Docherty, K. S., Worsnop, D. R., and Jimenez,  
568 J. L.: Field-deployable, high-resolution, time-of-flight aerosol mass spectrometer,  
569 *Anal. Chem.*, 78, 8281-8289, doi: 10.1021/ac061249n, 2006.

570 Ding, X., Zhang, Y.-Q., He, Q.-F., Yu, Q.-Q., Wang, J.-Q., Shen, R.-Q., Song, W., Wang,  
571 Y.-S., and Wang, X.-M.: Significant increase of aromatics-derived secondary  
572 organic aerosol during fall to winter in China, *Environ. Sci. Technol.*, 51, 7432-  
573 7441, doi: 10.1021/acs.est.6b06408, 2017.

574 **Drewnck, F., Hings, S. S., DeCarlo, P., Jayne, J. T., Gonin, M., Fuhrer, K., Weimer, S.,**  
575 **Jimenez, J. L., Demerjian, K. L., Borrmann, S., and Worsnop, D. R.: A new time-**  
576 **of-flight aerosol mass spectrometer (TOF-AMS)-instrument description and first**  
577 **field deployment, *Aerosol Sci. Technol.*, 39, 637-658, doi:**  
578 **10.1080/02786820500182040, 2005.**

579 Duporté, G., Parshintsev, J., Barreira, L. M. F., Hartonen, K., Kulmala, M., and  
580 Riekkola, M.-L.: Nitrogen-containing low volatile compounds from  
581 pinonaldehyde-dimethylamine reaction in the atmosphere: A laboratory and field  
582 study, *Environ. Sci. Technol.*, 50, 4693-4700, doi: 10.1021/acs.est.6b00270, 2016.

583 El Zein, A., Coeur, C., Obeid, E., Lauraguais, A., and Fagniez, T.: Reaction kinetics of  
584 catechol (1,2-benzenediol) and guaiacol (2-methoxyphenol) with ozone, *J. Phys.*  
585 *Chem. A*, 119, 6759-6765, doi: 10.1021/acs.jpca.5b00174, 2015.

586 Fang, J., Fu, Y., and Shang, C.: The roles of reactive species in micropollutant  
587 degradation in the UV/free chlorine system, *Environ. Sci. Technol.*, 48, 1859-1868,  
588 doi: 10.1021/es4036094, 2014.

589 **Farmer, D. K., Matsunaga, A., Docherty, K. S., Surratt, J. D., Seinfeld, J. H., Ziemann,**  
590 **P. J., and Jimenez, J. L.: Response of an aerosol mass spectrometer to**  
591 **organonitrates and organosulfates and implications for atmospheric chemistry,**  
592 ***Proc. Natl. Acad. Sci. U. S. A.*, 107, 6670-6675, doi: 10.1073/pnas.0912340107,**  
593 **2010.**

594 Ge, S., Xu, Y., and Jia, L.: Effects of inorganic seeds on secondary organic aerosol  
595 formation from photochemical oxidation of acetone in a chamber, *Atmos. Environ.*,  
596 170, 205-215, doi: 10.1016/j.atmosenv.2017.09.036, 2017a.

597 Ge, S., Xu, Y., and Jia, L.: Secondary organic aerosol formation from propylene  
598 irradiations in a chamber study, *Atmos. Environ.*, 157, 146-155, doi:  
599 10.1016/j.atmosenv.2017.03.019, 2017b.

600 Gordon, T. D., Presto, A. A., Nguyen, N. T., Robertson, W. H., Na, K., Sahay, K. N.,  
601 Zhang, M., Maddox, C., Rieger, P., Chattopadhyay, S., Maldonado, H., Maricq, M.  
602 M., and Robinson, A. L.: Secondary organic aerosol production from diesel  
603 vehicle exhaust: impact of aftertreatment, fuel chemistry and driving cycle, *Atmos.*  
604 *Chem. Phys.*, 14, 4643-4659, doi: 10.5194/acp-14-4643-2014, 2014.

605 Gysel, M., Weingartner, E., and Baltensperger, U.: Hygroscopicity of aerosol particles

606 at low temperatures. 2. Theoretical and experimental hygroscopic properties of  
607 laboratory generated aerosols, *Environ. Sci. Technol.*, 36, 63-68, doi:  
608 10.1021/es010055g, 2002.

609 Han, T., Liu, X., Zhang, Y., Qu, Y., Zeng, L., Hu, M., and Zhu, T.: Role of secondary  
610 aerosols in haze formation in summer in the Megacity Beijing, *J. Environ. Sci.*, 31,  
611 51-60, doi: 10.1016/j.jes.2014.08.026, 2015.

612 Hawthorne, S. B., Krieger, M. S., Miller, D. J., and Mathiason, M. B.: Collection and  
613 quantitation of methoxylated phenol tracers for atmospheric pollution from  
614 residential wood stoves, *Environ. Sci. Technol.*, 23, 470-475, doi:  
615 10.1021/es00181a013, 1989.

616 Hawthorne, S. B., Miller, D. J., Langenfeld, J. J., and Krieger, M. S.: PM10 high-  
617 volume collection and quantitation of semivolatile and nonvolatile phenols,  
618 methoxylated phenols, alkanes, and polycyclic aromatic hydrocarbons from winter  
619 urban air and their relationship to wood smoke emissions, *Environ. Sci. Technol.*,  
620 26, 2251-2262, doi: 10.1021/es00035a026, 1992.

621 Huang, D. D., Li, Y. J., Lee, B. P., and Chan, C. K.: Analysis of organic sulfur  
622 compounds in atmospheric aerosols at the HKUST supersite in Hong Kong using  
623 HR-ToF-AMS, *Environ. Sci. Technol.*, 49, 3672-3679, doi: 10.1021/es5056269,  
624 2015.

625 Huang, D. D., Zhang, X., Dalleska, N. F., Lignell, H., Coggon, M. M., Chan, C.-M.,  
626 Flagan, R. C., Seinfeld, J. H., and Chan, C. K.: A note on the effects of inorganic  
627 seed aerosol on the oxidation state of secondary organic aerosol-alpha-Pinene  
628 ozonolysis, *J. Geophys. Res.-Atmos.*, 121, 12476-12483, doi:  
629 10.1002/2016jd025999, 2016.

630 Huang, M., Hao, L., Gu, X., Hu, C., Zhao, W., Wang, Z., Fang, L., and Zhang, W.:  
631 Effects of inorganic seed aerosols on the growth and chemical composition of  
632 secondary organic aerosol formed from OH-initiated oxidation of toluene, *J.*  
633 *Atmos. Chem.*, 70, 151-164, doi: 10.1007/s10874-013-9262-9, 2013.

634 Huang, M., Hao, L., Cai, S., Gu, X., Zhang, W., Hu, C., Wang, Z., Fang, L., and Zhang,  
635 W.: Effects of inorganic seed aerosols on the particulate products of aged 1,3,5-  
636 trimethylbenzene secondary organic aerosol, *Atmos. Environ.*, 152, 490-502, doi:  
637 10.1016/j.atmosenv.2017.01.010, 2017.

638 Jaoui, M., Edney, E. O., Kleindienst, T. E., Lewandowski, M., Offenber, J. H., Surratt,  
639 J. D., and Seinfeld, J. H.: Formation of secondary organic aerosol from irradiated  
640 alpha-pinene/toluene/NO<sub>x</sub> mixtures and the effect of isoprene and sulfur dioxide,  
641 *J. Geophys. Res.-Atmos.*, 113, doi: 10.1029/2007jd009426, 2008.

642 Jimenez, J. L., Jayne, J. T., Shi, Q., Kolb, C. E., Worsnop, D. R., Yourshaw, I., Seinfeld,  
643 J. H., Flagan, R. C., Zhang, X., Smith, K. A., Morris, J. W., and Davidovits, P.:  
644 Ambient aerosol sampling using the Aerodyne Aerosol Mass Spectrometer, *J.*  
645 *Geophys. Res.-Atmos.*, 108, doi:10.1029/2001JD001213, 2003.

646 Kang, E., Root, M. J., Toohey, D. W., and Brune, W. H.: Introducing the concept of  
647 Potential Aerosol Mass (PAM), *Atmos. Chem. Phys.*, 7, 5727-5744, doi:

648 10.5194/acp-7-5727-2007, 2007.

649 Kleindienst, T. E., Edney, E. O., Lewandowski, M., Offenberg, J. H., and Jaoui, M.:

650 Secondary organic carbon and aerosol yields from the irradiations of isoprene and

651 alpha-pinene in the presence of NO<sub>x</sub> and SO<sub>2</sub>, *Environ. Sci. Technol.*, 40, 3807-

652 3812, doi: 10.1021/es052446r, 2006.

653 Krapf, M., El Haddad, I., Bruns, E. A., Molteni, U., Daellenbach, K. R., Prevot, A. S.

654 H., Baltensperger, U., and Dommen, J.: Labile peroxides in secondary organic

655 aerosol, *Chem*, 1, 603-616, doi: 10.1016/j.chempr.2016.09.007, 2016.

656 Kroll, J. H., Chan, A. W. H., Ng, N. L., Flagan, R. C., and Seinfeld, J. H.: Reactions of

657 semivolatile organics and their effects on secondary organic aerosol formation,

658 *Environ. Sci. Technol.*, 41, 3545-3550, doi: 10.1021/es062059x, 2007.

659 Kroll, J. H., Donahue, N. M., Jimenez, J. L., Kessler, S. H., Canagaratna, M. R., Wilson,

660 K. R., Altieri, K. E., Mazzoleni, L. R., Wozniak, A. S., Bluhm, H., Mysak, E. R.,

661 Smith, J. D., Kolb, C. E., and Worsnop, D. R.: Carbon oxidation state as a metric

662 for describing the chemistry of atmospheric organic aerosol, *Nature Chem.*, 3, 133-

663 139, doi: 10.1038/nchem.948, 2011.

664 Lauraguais, A., Coeur-Tourneur, C., Cassez, A., and Seydi, A.: Rate constant and

665 secondary organic aerosol yields for the gas-phase reaction of hydroxyl radicals

666 with syringol (2,6-dimethoxyphenol), *Atmos. Environ.*, 55, 43-48, doi:

667 10.1016/j.atmosenv.2012.02.027, 2012.

668 Lauraguais, A., Bejan, I., Barnes, I., Wiesen, P., Coeur-Tourneur, C., and Cassez, A.:

669 Rate coefficients for the gas-phase reaction of chlorine atoms with a series of

670 methoxylated aromatic compounds, *J. Phys. Chem. A*, 118, 1777-1784, doi:

671 10.1021/jp4114877, 2014a.

672 Lauraguais, A., Coeur-Tourneur, C., Cassez, A., Deboudt, K., Fourmentin, M., and

673 Choel, M.: Atmospheric reactivity of hydroxyl radicals with guaiacol (2-

674 methoxyphenol), a biomass burning emitted compound: Secondary organic

675 aerosol formation and gas-phase oxidation products, *Atmos. Environ.*, 86, 155-163,

676 doi: 10.1016/j.atmosenv.2013.11.074, 2014b.

677 Lauraguais, A., El Zein, A., Coeur, C., Obeid, E., Cassez, A., Rayez, M.-T., and Rayez,

678 J.-C.: Kinetic study of the gas-phase reactions of nitrate radicals with

679 methoxyphenol compounds: Experimental and theoretical approaches, *J. Phys.*

680 *Chem. A*, 120, 2691-2699, doi: 10.1021/acs.jpca.6b02729, 2016.

681 Lelieveld, J., Crutzen, P. J., Ramanathan, V., Andreae, M. O., Brenninkmeijer, C. A. M.,

682 Campos, T., Cass, G. R., Dickerson, R. R., Fischer, H., de Gouw, J. A., Hansel, A.,

683 Jefferson, A., Kley, D., de Laat, A. T. J., Lal, S., Lawrence, M. G., Lobert, J. M.,

684 Mayol-Bracero, O. L., Mitra, A. P., Novakov, T., Oltmans, S. J., Prather, K. A.,

685 Reiner, T., Rodhe, H., Scheeren, H. A., Sikka, D., and Williams, J.: The Indian

686 Ocean Experiment: Widespread air pollution from South and Southeast Asia,

687 *Science*, 291, 1031-1036, doi: 10.1126/science.1057103, 2001.

688 Li, H., Zhang, Q., Zhang, Q., Chen, C., Wang, L., Wei, Z., Zhou, S., Parworth, C., Zheng,

689 B., Canonaco, F., Prevot, A. S. H., Chen, P., Zhang, H., Wallington, T. J., and He,

690 K.: Wintertime aerosol chemistry and haze evolution in an extremely polluted city  
691 of the North China Plain: Significant contribution from coal and biomass  
692 combustion, *Atmos. Chem. Phys.*, 17, 4751-4768, doi: 10.5194/acp-17-4751-2017,  
693 2017.

694 **Liggio, J., Li, S.-M., and McLaren, R.: Reactive uptake of glyoxal by particulate matter,**  
695 ***J. Geophys. Res.-Atmos.*, 110, doi:10.1029/2004JD005113, 2005.**

696 Lin, Y. H., Knipping, E. M., Edgerton, E. S., Shaw, S. L., and Surratt, J. D.:  
697 Investigating the influences of SO<sub>2</sub> and NH<sub>3</sub> levels on isoprene-derived secondary  
698 organic aerosol formation using conditional sampling approaches, *Atmos. Chem.*  
699 *Phys.*, 13, 8457–8470, doi: 10.5194/acp-13-8457-2013, 2013.

700 Liu, J., Lin, P., Laskin, A., Laskin, J., Kathmann, S. M., Wise, M., Caylor, R., Imholt,  
701 F., Selimovic, V., and Shilling, J. E.: Optical properties and aging of light-  
702 absorbing secondary organic aerosol, *Atmos. Chem. Phys.*, 16, 12815-12827, doi:  
703 10.5194/acp-16-12815-2016, 2016a.

704 Liu, T., Wang, X., Hu, Q., Deng, W., Zhang, Y., Ding, X., Fu, X., Bernard, F., Zhang,  
705 Z., Lu, S., He, Q., Bi, X., Chen, J., Sun, Y., Yu, J., Peng, P., Sheng, G., and Fu, J.:  
706 Formation of secondary aerosols from gasoline vehicle exhaust when mixing with  
707 SO<sub>2</sub>, *Atmos. Chem. Phys.*, 16, 675-689, doi: 10.5194/acp-16-675-2016, 2016b.

708 **Liu, Z., Ge, M., Yin, S., and Wang, W.: Uptake and reaction kinetics of  $\alpha$ -pinene and  $\beta$ -**  
709 **pinene with sulfuric acid solutions, *Chem. Phys. Lett.*, 491, 146-150, doi:**  
710 **10.1016/j.cplett.2010.04.004, 2010.**

711 Marais, E. A., Jacob, D. J., Turner, J. R., and Mickley, L. J.: Evidence of 1991-2013  
712 decrease of biogenic secondary organic aerosol in response to SO<sub>2</sub> emission  
713 controls, *Environ. Res. Lett.*, 12, doi: 10.1088/1748-9326/aa69c8, 2017.

714 Meade, L. E., Riva, M., Blomberg, M. Z., Brock, A. K., Qualters, E. M., Siejack, R. A.,  
715 Ramakrishnan, K., Surratt, J. D., and Kautzman, K. E.: Seasonal variations of fine  
716 particulate organosulfates derived from biogenic and anthropogenic hydrocarbons  
717 in the mid-Atlantic United States, *Atmos. Environ.*, 145, 405-414, doi:  
718 10.1016/j.atmosenv.2016.09.028, 2016.

719 Mielke, L. H., Furgeson, A., and Osthoff, H. D.: Observation of ClNO<sub>2</sub> in a mid-  
720 continental urban environment, *Environ. Sci. Technol.*, 45, 8889-8896, doi:  
721 10.1021/es201955u, 2011.

722 Naeher, L. P., Brauer, M., Lipsett, M., Zelikoff, J. T., Simpson, C. D., Koenig, J. Q., and  
723 Smith, K. R.: Woodsmoke health effects: A review, *Inhal. Toxicol.*, 19, 67-106, doi:  
724 10.1080/08958370600985875, 2007.

725 Ng, N. L., Chhabra, P. S., Chan, A. W. H., Surratt, J. D., Kroll, J. H., Kwan, A. J.,  
726 McCabe, D. C., Wennberg, P. O., Sorooshian, A., Murphy, S. M., Dalleska, N. F.,  
727 Flagan, R. C., and Seinfeld, J. H.: Effect of NO<sub>x</sub> level on secondary organic aerosol  
728 (SOA) formation from the photooxidation of terpenes, *Atmos. Chem. Phys.*, 7,  
729 5159-5174, doi: 10.5194/acp-7-5159-2007, 2007.

730 Ng, N. L., Canagaratna, M. R., Jimenez, J. L., Chhabra, P. S., Seinfeld, J. H., and  
731 Worsnop, D. R.: Changes in organic aerosol composition with aging inferred from

732 aerosol mass spectra, *Atmos. Chem. Phys.*, 11, 6465-6474, doi: 10.5194/acp-11-  
733 6465-2011, 2011.

734 Nolte, C. G., Schauer, J. J., Cass, G. R., and Simoneit, B. R. T.: Highly polar organic  
735 compounds present in wood smoke and in the ambient atmosphere, *Environ. Sci.*  
736 *Technol.*, 35, 1912-1919, doi: 10.1021/es001420r, 2001.

737 O'Neill, E. M., Kawam, A. Z., Van Ry, D. A., and Hinrichs, R. Z.: Ozonolysis of surface-  
738 adsorbed methoxyphenols: kinetics of aromatic ring cleavage vs. alkene side-chain  
739 oxidation, *Atmos. Chem. Phys.*, 14, 47-60, doi: 10.5194/acp-14-47-2014, 2014.

740 Odum, J. R., Hoffmann, T., Bowman, F., Collins, D., Flagan, R. C., and Seinfeld, J. H.:  
741 Gas/particle partitioning and secondary organic aerosol yields, *Environ. Sci.*  
742 *Technol.*, 30, 2580-2585, doi: 10.1021/es950943+, 1996.

743 Park, J.-H., Ivanov, A. V., and Molina, M. J.: Effect of relative humidity on OH uptake  
744 by surfaces of atmospheric importance, *J. Phys. Chem. A*, 112, 6968-6977, doi:  
745 10.1021/jp8012317, 2008.

746 Riva, M., Tomaz, So, Cui, T., Lin, Y. H., Perraudin, E., Gold, A., Stone, E. A., Villenave,  
747 E., and Surratt, J. D.: Evidence for an unrecognized secondary anthropogenic  
748 source of organosulfates and sulfonates: Gas-phase oxidation of polycyclic  
749 aromatic hydrocarbons in the presence of sulfate aerosol, *Environ. Sci. Technol.*,  
750 49, 6654–6664, doi: 10.1021/acs.est.5b00836, 2015.

751 Sarrafzadeh, M., Wildt, J., Pullinen, I., Springer, M., Kleist, E., Tillmann, R., Schmitt,  
752 S. H., Wu, C., Mentel, T. F., Zhao, D., Hastie, D. R., and Kiendler-Scharr, A.:  
753 Impact of NO<sub>x</sub> and OH on secondary organic aerosol formation from beta-pinene  
754 photooxidation, *Atmos. Chem. Phys.*, 16, 11237-11248, doi: 10.5194/acp-16-  
755 11237-2016, 2016.

756 Sato, K., Takami, A., Isozaki, T., Hikida, T., Shimono, A., and Imamura, T.: Mass  
757 spectrometric study of secondary organic aerosol formed from the photo-oxidation  
758 of aromatic hydrocarbons, *Atmos. Environ.*, 44, 1080-1087, doi:  
759 10.1016/j.atmosenv.2009.12.013, 2010.

760 Schauer, J. J., Kleeman, M. J., Cass, G. R., and Simoneit, B. R. T.: Measurement of  
761 emissions from air pollution sources. 3. C-1-C-29 organic compounds from  
762 fireplace combustion of wood, *Environ. Sci. Technol.*, 35, 1716-1728, doi:  
763 10.1021/es001331e, 2001.

764 Simoneit, B. R. T., Rogge, W. F., Mazurek, M. A., Standley, L. J., Hildemann, L. M.,  
765 and Cass, G. R.: Lignin pyrolysis products, lignans, and resin acid as specific  
766 tracers of plant classes in emissions from biomass combustion, *Environ. Sci.*  
767 *Technol.*, 27, 2533-2541, doi: 10.1021/es00048a034, 1993.

768 Takekawa, H., Minoura, H., and Yamazaki, S.: Temperature dependence of secondary  
769 organic aerosol formation by photo-oxidation of hydrocarbons, *Atmos. Environ.*,  
770 37, 3413-3424, doi: 10.1016/s1352-2310(03)00359-5, 2003.

771 Ulbrich, I. M., Canagaratna, M. R., Zhang, Q., Worsnop, D. R., and Jimenez, J. L.:  
772 Interpretation of organic components from Positive Matrix Factorization of  
773 aerosol mass spectrometric data, *Atmos. Chem. Phys.*, 9, 2891-2918, doi:

774 10.5194/acp-9-2891-2009, 2009.  
775 Weis, D. D., and Ewing, G. E.: Water content and morphology of sodium chloride  
776 aerosol particles, *J. Geophys. Res.-Atmos.*, 104, 21275-21285, doi:  
777 10.1029/1999jd900286, 1999.  
778 Xu, L., Middlebrook, A. M., Liao, J., de Gouw, J. A., Guo, H., Weber, R. J., Nenes, A.,  
779 Lopez-Hilfiker, F. D., Lee, B. H., Thornton, J. A., Brock, C. A., Neuman, J. A.,  
780 Nowak, J. B., Pollack, I. B., Welti, A., Graus, M., Warneke, C., and Ng, N. L.:  
781 Enhanced formation of isoprene-derived organic aerosol in sulfur-rich power plant  
782 plumes during Southeast Nexus, *J. Geophys. Res.-Atmos.*, 121, 11137-11153, doi:  
783 10.1002/2016jd025156, 2016.  
784 Yang, B., Zhang, H., Wang, Y., Zhang, P., Shu, J., Sun, W., and Ma, P.: Experimental  
785 and theoretical studies on gas-phase reactions of NO<sub>3</sub> radicals with three  
786 methoxyphenols: Guaiacol, creosol, and syringol, *Atmos. Environ.*, 125, 243-251,  
787 doi: 10.1016/j.atmosenv.2015.11.028, 2016.  
788 Ye, J., Abbatt, J. P. D., and Chan, A. W. H.: Novel pathway of SO<sub>2</sub> oxidation in the  
789 atmosphere: reactions with monoterpene ozonolysis intermediates and secondary  
790 organic aerosol, *Atmos. Chem. Phys.*, 18, 5549-5565, doi: 10.5194/acp-18-5549-  
791 2018, 2018.  
792 Yee, L. D., Kautzman, K. E., Loza, C. L., Schilling, K. A., Coggon, M. M., Chhabra, P.  
793 S., Chan, M. N., Chan, A. W. H., Hersey, S. P., Crouse, J. D., Wennberg, P. O.,  
794 Flagan, R. C., and Seinfeld, J. H.: Secondary organic aerosol formation from  
795 biomass burning intermediates: Phenol and methoxyphenols, *Atmos. Chem. Phys.*,  
796 13, 8019-8043, doi: 10.5194/acp-13-8019-2013, 2013.  
797 Zhang, X., Cappa, C. D., Jathar, S. H., McVay, R. C., Ensberg, J. J., Kleeman, M. J.,  
798 and Seinfeld, J. H.: Influence of vapor wall loss in laboratory chambers on yields  
799 of secondary organic aerosol, *Proc. Natl. Acad. Sci. U. S. A.*, 111, 5802-5807, doi:  
800 10.1073/pnas.1404727111, 2014.  
801 Zhang, X., Schwantes, R. H., McVay, R. C., Lignell, H., Coggon, M. M., Flagan, R. C.,  
802 and Seinfeld, J. H.: Vapor wall deposition in Teflon chambers, *Atmos. Chem. Phys.*,  
803 15, 4197-4214, doi: 10.5194/acp-15-4197-2015, 2015.

804 **Table 1.** Experimental **conditions** and results for guaiacol photooxidation in the presence

805 NO<sub>x</sub>.

Exp.	[Guaiacol] <sub>0</sub> (μg m <sup>-3</sup> )	Δ[Guaiacol] (μg m <sup>-3</sup> ) <sup>a</sup>	[NO <sub>x</sub> ] <sub>0</sub> (ppbv)	[NO] <sub>0</sub> (ppbv)	RH (%)	T (K)	M <sub>0</sub> (μg m <sup>-3</sup> ) <sup>b</sup>	Yield (%)
1	136.83	112.34	25.1	13.2	39	302	10.63 ± 0.65	9.46 ± 1.71
2	309.06	282.33	52.7	34.4	38	302	34.72 ± 0.94	12.30 ± 0.98
3	375.19	335.94	58.3	44.5	40	302	63.62 ± 1.71	18.94 ± 1.49
4	718.49	613.25	116.7	98.5	38	302	130.19 ± 3.28	21.23 ± 1.56
5	1321.25	1116.20	209.2	184.1	39	302	256.88 ± 6.69	23.01 ± 1.75
6	1470.66	1175.03	248	200	38	302	297.65 ± 8.85	25.33 ± 2.21
7	2197.36	1664.29	335	286	38	302	438.82 ± 10.25	26.37 ± 2.83

806 <sup>a</sup> The consumed guaiacol concentration at the end of each experiment.

807 <sup>b</sup> M<sub>0</sub> is the mass concentration of SOA.

808 **Table 2.** Experimental **conditions** and results for guaiacol photooxidation in the presence of seed particles and SO<sub>2</sub>.

Exp.	[Guaiacol] <sub>0</sub> (μg m <sup>-3</sup> )	Δ[Guaiacol] (μg m <sup>-3</sup> ) <sup>a</sup>	Seed	[SO <sub>2</sub> ] <sub>0</sub> (ppbv)	[NO <sub>x</sub> ] <sub>0</sub> (ppbv)	[NO] <sub>0</sub> (ppbv)	RH (%)	T (K)	N <sub>s</sub> (m <sup>-3</sup> ) <sup>b</sup>	D <sub>s</sub> (nm) <sup>c</sup>	C <sub>seed</sub> (μg m <sup>-3</sup> ) <sup>d</sup>	C <sub>sulfate</sub> (μg m <sup>-3</sup> ) <sup>e</sup>	S <sub>0</sub> (μm <sup>2</sup> cm <sup>-3</sup> ) <sup>f</sup>	S <sub>f</sub> (μm <sup>2</sup> cm <sup>-3</sup> ) <sup>g</sup>	$\bar{\tau}_{g-p} / \tau_{g-w}$ <sup>h</sup>	M <sub>0</sub> (μg m <sup>-3</sup> ) <sup>i</sup>	Yield (%)	OS <sub>C</sub> <sup>j</sup>
1	375.19	335.94	–	–	58.3	44.5	40	302	–	–	–	–	–	1.25 × 10 <sup>3</sup>	0.82	63.62 ± 1.71	18.94 ± 1.49	0.11 ± 0.007
2	363.53	332.79	–	33	54.5	37.4	38	302	–	–	–	7.42	–	1.68 × 10 <sup>3</sup>	0.71	71.88 ± 1.43	21.60 ± 1.27	0.14 ± 0.006
3	370.12	335.58	–	56	57.3	41.8	38	302	–	–	–	17.89	–	2.04 × 10 <sup>3</sup>	0.61	78.59 ± 2.06	23.42 ± 1.80	0.18 ± 0.006
4	379.05	346.03	NaCl	–	58.8	40.7	39	302	10700	56	15.63	–	2.69 × 10 <sup>2</sup>	1.47 × 10 <sup>3</sup>	0.54	84.91 ± 2.01	24.54 ± 1.73	0.29 ± 0.007
5	378.44	339.34	NaCl	30	57.4	41.9	38	302	11300	58	13.84	7.51	2.64 × 10 <sup>2</sup>	2.32 × 10 <sup>3</sup>	0.43	90.89 ± 2.28	26.78 ± 1.97	0.30 ± 0.008
6	380.77	340.15	NaCl	54	60.1	46.1	39	301	11200	56	14.28	16.67	2.81 × 10 <sup>2</sup>	2.91 × 10 <sup>3</sup>	0.35	98.86 ± 2.11	29.06 ± 1.82	0.33 ± 0.008
7	373.57	340.86	(NH <sub>4</sub> ) <sub>2</sub> SO <sub>4</sub>	–	58.3	42.6	39	302	10400	53	15.45	–	2.75 × 10 <sup>2</sup>	1.53 × 10 <sup>3</sup>	0.62	79.44 ± 1.86	23.31 ± 1.59	0.20 ± 0.006
8	376.26	343.19	(NH <sub>4</sub> ) <sub>2</sub> SO <sub>4</sub>	33	56.8	38.9	38	302	10100	53	14.38	7.84	2.80 × 10 <sup>2</sup>	2.57 × 10 <sup>3</sup>	0.53	84.35 ± 2.09	24.58 ± 1.78	0.22 ± 0.007
9	381.33	341.01	(NH <sub>4</sub> ) <sub>2</sub> SO <sub>4</sub>	54	57.8	39.2	38	303	10700	51	14.90	17.25	2.82 × 10 <sup>2</sup>	3.10 × 10 <sup>3</sup>	0.44	89.92 ± 2.31	26.37 ± 1.98	0.23 ± 0.004

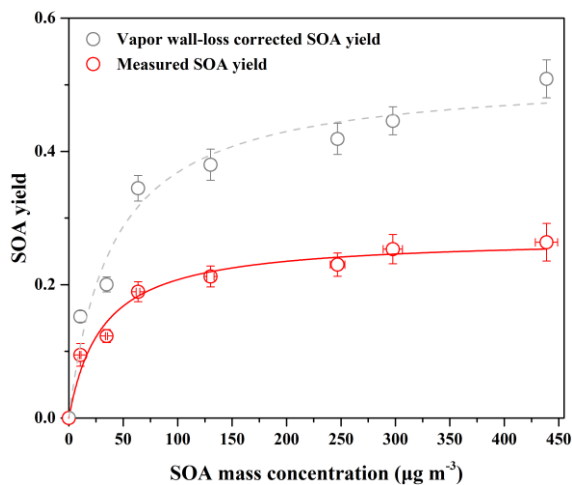
809 <sup>a</sup> The consumed guaiacol concentration at the end of each experiment. <sup>b</sup> N<sub>s</sub> is the initial seed number. <sup>c</sup> D<sub>s</sub> is the average diameter of seed particles.

810 <sup>d</sup> C<sub>seed</sub> is the initial concentration of seed. <sup>e</sup> C<sub>sulfate</sub> is the sulfate concentration formed by SO<sub>2</sub> oxidation. <sup>f</sup> The initial surface area of seed particles.

811 <sup>g</sup> The final surface area of aerosol particles (seed + organic aerosol), measured by the SMPS. <sup>h</sup> The ratio of the average gas-particle partitioning

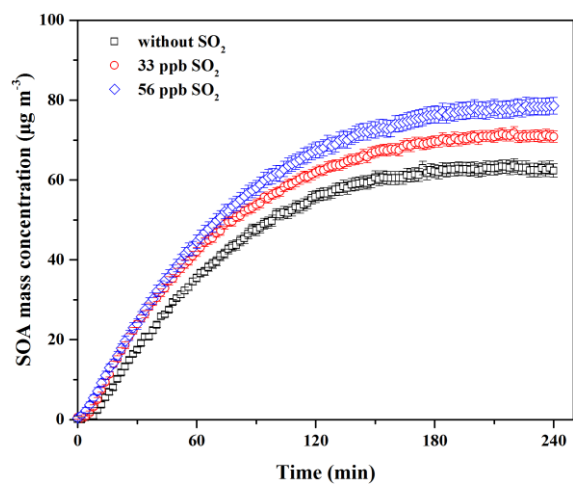
812 timescale ( $\bar{\tau}_{g-p}$ ) over the course of experiment to the vapor wall deposition timescale ( $\tau_{g-w}$ ). <sup>i</sup> M<sub>0</sub> is the mass concentration of SOA. <sup>j</sup> OS<sub>C</sub> is the

813 average oxidation state of carbon of SOA.



814

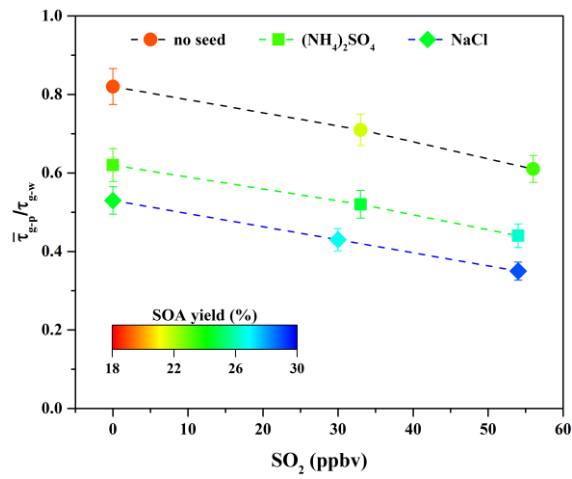
815 **Figure 1.** SOA yield as a function of SOA mass concentration ( $M_o$ ) for guaiacol  
 816 photooxidation in the presence of  $\text{NO}_x$  at different guaiacol concentrations. The solid  
 817 lines was fit to the experimental data using a one-product model. Values of  $\alpha$  and  $K_{om,i}$   
 818 used to generate the solid line were  $(0.27 \pm 0.01)$  and  $(0.033 \pm 0.008)$ , and their values  
 819 for the dot line were  $(0.52 \pm 0.03)$  and  $(0.025 \pm 0.006)$ , respectively.



820

821 **Figure 2.** Time-dependent growth curves of SOA mass concentration for guaiacol

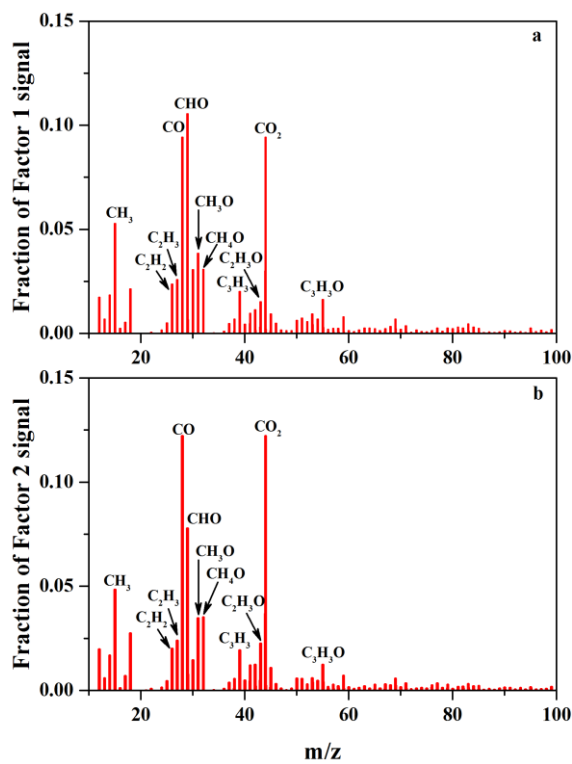
822 photooxidation at different SO<sub>2</sub> levels (Exps. 1–3 in Table 2).



823

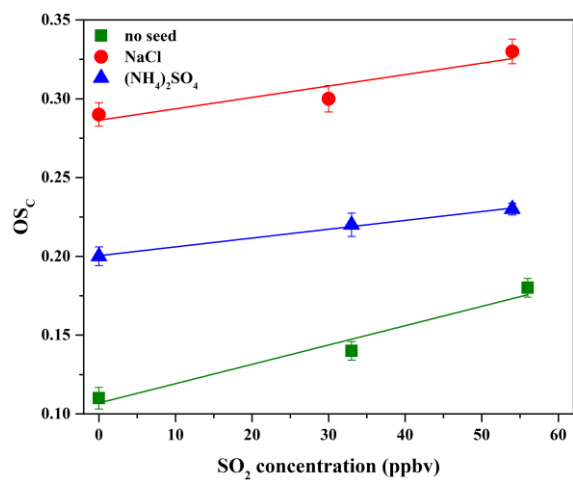
824 **Figure 3.** Variations in  $\bar{\tau}_{g-p} / \tau_{g-w}$  ratio in the presence of various seed particles as a

825 function of  $SO_2$  concentration.



826

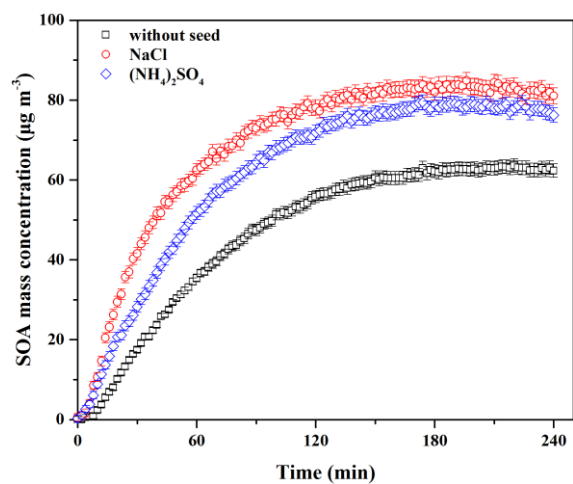
827 **Figure 4.** Mass spectra of Factor 1 (a) and Factor 2 (b) for the formed SOA identified  
 828 by applying PMF analysis to the AMS data, **obtained at different SO<sub>2</sub> concentrations**  
 829 **over the course of experiments.**



830

831 **Figure 5.** OSC of SOA formed in the presence of various seed particles as a function of

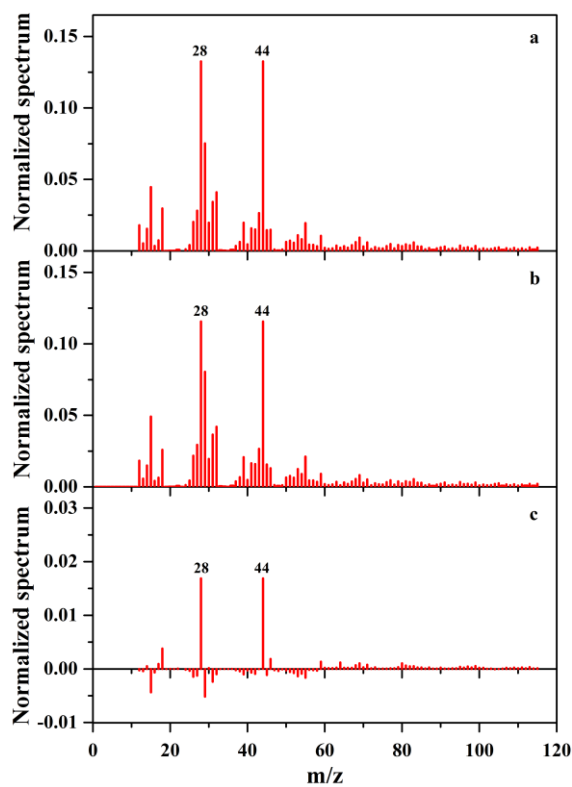
832 SO<sub>2</sub> concentration.



833

834 **Figure 6.** Time-dependent growth curves of SOA mass concentration for guaiacol

835 photooxidation in the presence of inorganic seed particles (Exps. 1, 4 and 7 in Table 2).

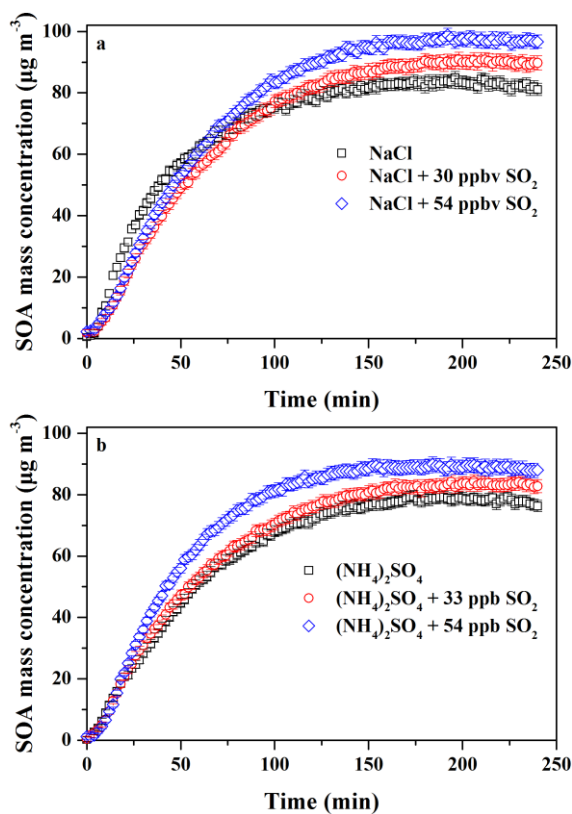


836

837 **Figure 7.** Mass spectra of SOA with NaCl (a) and (NH<sub>4</sub>)<sub>2</sub>SO<sub>4</sub> (b) as seed particles

838 obtained by the HR-ToF-AMS, as well as their difference mass spectrum (c) obtained

839 by a minus b.



840

841 **Figure 8.** Time-dependent growth curves of SOA mass concentration for guaiacol

842 photooxidation in the presence of  $\text{SO}_2$  and inorganic seed particles (a: NaCl; b:

843  $(\text{NH}_4)_2\text{SO}_4$ ) (Exps. 4–9 in Table 2).